Numerical and Experimental Assessment of the New Magnetic Field Configuration in SPIDER

Nicolò Marconato, Emanuele Sartori, and Gianluigi Serianni

***Abstract*— Magnetic field plays an essential role in negative ion-driven neutral beam injectors (NBIs), being necessary to counteract the inevitable interaction between electrons and negative ions, both to maximize the ion production and to minimize the electron extraction and acceleration. Magnetic field influences also the generation and confinement of the plasma from where the ions are extracted, and this is particularly significant for radio frequency (RF) inductively generated plasmas, such as the case of SPIDER. SPIDER is the full-scale prototype of the ITER NBI ion source, in operation since 2018. Its magnetic field configuration was modified in 2020 to solve issues related to plasma generation. The new configuration has significantly improved the performances, but some limitations and lack of symmetries emerge at high field. The present article describes the numerical and experimental assessment recently carried out in order to verify the actual distribution of the new magnetic field configuration inside the SPIDER ion source and accelerator, and to investigate on possible reasons of asymmetries.**

***Index Terms*— Finite element model (FEM), magnetic confinement fusion, magnetic filter field (FF), magnetic topology, neutral beam injector (NBI).**

I. Introduction

NEGATIVE ion driven neutral beam injectors (NBIs) require a complex magnetic field structure inside the ion source and accelerator region, with two basic purposes: filter out the electrons from the region where the negative ions are produced, extracted, and accelerated, and confine the plasma in order to reduce losses at the walls [1]–[7]. The fulfillment of both requirements at the same time is not straightforward, different magnetic field sources are required which unavoidably interplay one to each other, making an optimum design complex. This is especially true for large size NBIs operating thanks to radio frequency (RF) generated plasmas, as it is the case of SPIDER, the full-scale prototype of the ITER NBI source [1], [6], [7]. As a matter of fact, the uniformity and intensity requirements on the magnetic field close to the plasma-facing electrode, which separates the source from the accelerator, may clash with those in the region of the RF drivers where the plasma is generated.

The magnetic field in SPIDER is produced by a combination of several sets of permanent magnets embedded in different components of the ion source and the accelerator, and by a dc (or slowly varying) electric current flowing in the plasma-facing electrode and closing in an assembly of bus-bars specifically positioned. This bus-bar system has been recently modified with respect to the original design [8] in order to improve the plasma confinement in the RF drivers, as a result of the first experimental evidences which showed a degradation of the plasma light strictly correlated with the magnetic field intensity [7], [8]. The improvement proved to be significant [9], [10], but the filter field (FF) intensity can still affect the operation of some RF drivers [8]; however, in the new configuration this occurs at a much higher field.

The present work describes the latest activities carried out, both numerically and experimentally, for a thorough investigation on the possible reasons of this behavior, which can be investigated in terms of the interplay among the different magnetic field sources. The possibility to further increase the FF while maintaining good plasma performances in the RF drivers would likely be beneficial for the NBI efficiency, in terms of reduced electron/ion extracted current.

This article is organized as follows: in Section II the SPIDER magnetic field sources are introduced; a measurement system for the routine verification of the current sharing among the different bus-bars and consequently of the FF distribution is described in Section III; details on a measurement campaign for mapping the magnetic field inside the ion source are given in Section IV; the numerical models of the whole field sources implemented is described in Section V; and finally conclusions are drawn in Section VI.

II. SPIDER Magnetic Field Sources

The magnetic field configuration in SPIDER is the result of a combination of different sources [11], shown in Fig. 1.

It is possible to make a basic distinction: one magnetic field source which can be varied during operation, generated by the electric current across a system of bus-bars [see Fig. 1(1)], and fixed field sources, made up of different sets of permanent magnets [see Fig. 1(2)].

A. Filter Field

The current generated magnetic field is usually referred to as magnetic FF. It is generated by an electric current flowing

Manuscript received 28 January 2022; revised 4 April 2022; accepted 9 April 2022. Date of publication 3 May 2022; date of current version 30 November 2022. This work was supported by the ITER Organization, carried out within the framework of the ITER-RFX Neutral Beam Testing Facility (NBTF) Agreement. The review of this article was arranged by Senior Editor G. H. Neilson. *(Corresponding author: Nicolò Marconato.)*

Nicolò Marconato is with the Consorzio RFX (CNR, ENEA, INFN, Università di Padova, Acciaierie Venete SpA), 35127 Padua, Italy, and also with the Department of Industrial Engineering (DII), University of Padua, 35131 Padua, Italy (e-mail: nicolo.marconato@igi.cnr.it).

Emanuele Sartori is with the Consorzio RFX (CNR, ENEA, INFN, Università di Padova, Acciaierie Venete SpA), 35127 Padua, Italy, and also with the Department of Engineering and Management, University of Padova, 36100 Vicenza, Italy.

Gianluigi Serianni is with the Consorzio RFX (CNR, ENEA, INFN, Università di Padova, Acciaierie Venete SpA), 35127 Padua, Italy.

Color versions of one or more figures i n this article are available at https://doi.org/10.1109/TPS.2022.3167859.

Digital Object Identifier 10.1109/TPS.2022.3167859

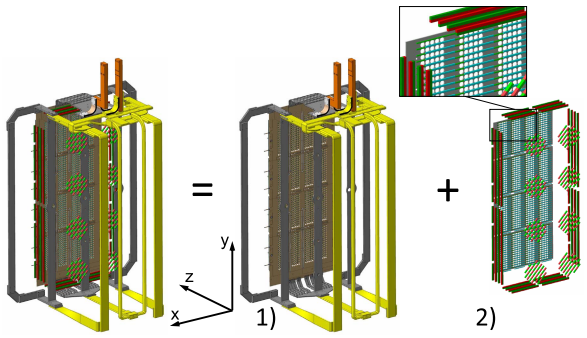

Fig. 1. CAD model of the magnetic field sources in SPIDER, made up of (1) PG current bus-bar system and (2) different permanent magnet sets.

in the plasma-facing grid electrode, also called plasma grid (PG), and in different bus-bars accurately positioned all around the plasma source. Therefore, it has a distribution spread all across the source and behind of it, with a main horizontal component parallel to the accelerator grids (B_x) and it has the main purpose of reducing the electron temperature and density in the vicinity of the PG, and hence improving the lifetime and density of negative ions. In particular, some of the bus-bars have been added at a later time in 2020 (highlighted in yellow in Fig. 1) and their connections to the old ones (highlighted in gray in Fig. 1) changed in order to modify the magnetic field topology inside the RF drivers, keeping as much unchanged as possible the field in proximity of the PG. The current can be varied between 0 and 5 kA during SPIDER operations, allowing to test the influence of the FF on the performances of the source plasma and of the ion beam. The additional bus-bars and their connections have been designed in such a way to modify the magnetic topology in the RF drivers, by changing the ratio between the current in the new (yellow) and in the original (gray) bars electrically in parallel. In order to easily modify the current sharing, without introducing other modification to the circuit, thin layers of graphite have been chosen as resistive elements to be inserted in between some bus-bar joints: by changing the thickness of the layer in one branch of the circuit with respect to the other, the current ratio between the two branches can be changed. This operation clearly requires dismounting some components during SPIDER shut-down. More details can be found in [8].

B. Plasma Confinement and Electron Deflection

Different sets of permanent magnets are embedded in the ion source and accelerator structures, some of them with plasma confinement purpose and other to filter out the co-extracted electrons. More precisely, four sets can be distinguished.

1) *Driver Back Plate Permanent Magnets (DBPMs):* A set of Samarium Cobalt magnets (RECOMA 22-B_r = 0.94 T) embedded inside each of the eight driver back plate, arranged in such a way to produce a chessboard-shaped cusp type magnetic configuration, with the aim to confine the plasma by limiting the electron losses on these walls.
2) *Lateral Wall Permanent Magnets (LWPMs):* A set of Samarium Cobalt magnets (RECOMA 22-B_r = 0.94 T) embedded in the lateral and top and bottom walls of the plasma source expansion box. It constitutes a frame made up by four rows of magnets alternately polarized toward the inside and outside of the chamber, in a cusp configuration, with the aim to confine the plasma by limiting the electron losses on these walls.
3) *Extraction Grid Permanent Magnets (EGPMs):* A set of Samarium Cobalt magnets (RECOMA 32s-B_r = 1.15 T) embedded in the second grid electrode, called extraction grid (EG), in rows between each aperture row (and above and below the extreme ones) and alternately polarized along the beam direction (z) and in the opposite, one row and the next. They produce a magnetic field mainly oriented along the vertical direction (B_y), upstream and downstream each EG aperture, alternately oriented upward and downward one row and the next, with the aim of deflecting the co-extracted electrons so as to make them impinge on the EG itself and thus avoid to further accelerate them.
4) *Compensation Permanent Magnets (CPMs):* A set of Samarium Cobalt magnets (RECOMA 5-B_r = 0.4 T) embedded in the third grid electrode, called grounded grid (GG), again polarized along the beam direction (z) and in the opposite, one row and the next, exactly reproducing the pattern of the EGPM. They have been introduced in order to compensate the "criss-cross" horizontal deflection of ion trajectories unavoidably introduced by the EGPM field [12].
5) A 4-mm-Thick Ferromagnetic Plate (Armco Steel) is installed on the downstream side of the GG, in direct contact with the CPM, so as to force the reclosure of the magnetic flux due to the CPMs inside of the iron, making the magnets generating a unidirectional field in front of the openings of the GG and thus allowing the deflection compensation. The presence of the iron plate also further limits the FF component parallel to the grids (B_x) in the accelerator and thus the vertical deflection of the ion beam.

III. PG Current Sharing Monitor

This measurement system is implemented in order to monitor the sharing of the FF current among the different return bus-bars. Indeed, a careful testing campaign was carried out before adopting graphite sheets as resistive elements to control the current distribution [8], but the novelty of the solution asked for a continuous online assessment of the current distribution. A measure of the current flowing in the three new bus-bars, each of them in parallel with the reciprocal original bus-bar, has been implemented by measuring the voltage drop along the vertical bus-bar sections. Known their resistance, it is easy to make the conversion between voltage and current. The voltage across the "resistive" joints with thicker graphite sheets was also kept under control, in order to verify potential anomalous behaviors.

In Fig. 2 the six top and the three bottom measurement locations are highlighted in a zoom view of the SPIDER CAD model showing the FF bus-bars.

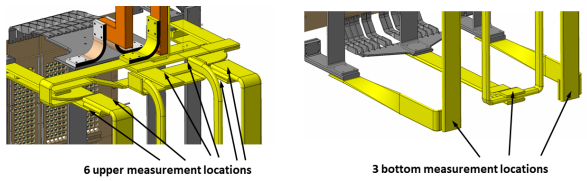

Fig. 2. Zoom view of the CAD model indicating the six top (left) and three bottom (right) measurement locations.

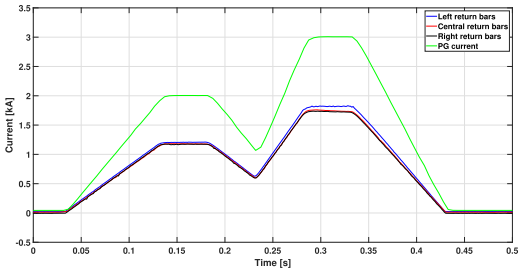

Fig. 3. FF current variation (green) during a dry shot and estimated currents in the three new branches of the return bus-bars.

The diagnostics requires the measurement of a potential difference of a few millivolts, collected on a high voltage system, at the source potential up to −100 kV. Therefore, the voltage references are brought out of the vacuum vessel with kapton wires connected to a vacuum tight electrical feed-through connected to a small pipe in the hydraulic bushing on the bottom side of SPIDER. The analog signals are then converted into optical through a battery-supplied electronic board specifically designed and positioned on a shelf behind the bushing at the source potential. It consists of three ADS1115, 16-b four-channel ADC with programmable gain amplifier, connected to an Arduino board which multiplexes the signals to an opto-converter. An optical fiber connects the high voltage part to a opto-digital conversion board connected to the acquisition system.

This system allows estimating the actual current in the different bus-bars, operation routinely carried out in the first dry test pulses of the day, during time interval when the RF generators are not operating, which would cause an unacceptable noise for this measurement. In Fig. 3, a typical waveform of the FF current (green) in one of these test pulses is shown, together with the estimated currents in the new return bus-bars, which correctly correspond to about 60% of the total current.

A maximum 5% left-right non-uniformity was measured (left +1%, right −4% with respect the theoretic 60% of the FF current).

IV. Magnetic Mapping Campaign

Current sharing measurements described above led to consider that the magnetic FF distribution corresponds to design. Nevertheless, results from high current operations, showing plasma instabilities in correspondence of the top and bottom driver locations on the right side of the machine, prompted an *ad hoc* measurement campaign in order to assess for possible unexpected non-uniformities. A system for mapping the magnetic field inside the expansion chamber was implemented. It consists of eight Hall sensors placed on the tip of plastic

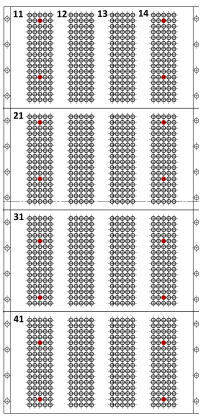

Fig. 4. Hall probe locations and beamlet group reference system.

Fig. 5. Picture of the positioning system for the hall probes fixed on the left and right locations.

sticks inserted through some apertures of the acceleration grids. The sticks are supported by an aluminum profile and fixed to the vertical locations corresponding to the apertures highlighted in red in Fig. 4 which sketches all the 1280 grid apertures.

Two horizontal positions were tested, corresponding to the central beamlets of the left and right external beamlet groups, as sketched in Fig. 4 and shown in Fig. 5, which reports a picture of the real system in the two positions tested. The system is designed to allow inserting the Hall probes inside the plasma source and sampling the magnetic field along a straight path between the PG and the driver exits. Rectangular elements were glued to the other end of the sticks in order to identify the orientation of the probes, as shown in Fig. 5.

It is worth introducing that from here on we will refer to the left and right sides of the source looking in the direction of the beam from behind the source. In other words, left corresponds to positive x and right to negative x coordinates in the reference system usually adopted and shown in Fig. 1 ($x = 0$ corresponds to the center of the grids).

In particular, the magnetic field was sampled at five locations inside the source on the left side, corresponding to the z coordinate at 10, 50, 100, 150, and 190 mm from the PG, and only at $z = 50$ and 150 mm on the right side. All measurements were taken during a shutdown with the vessel open and thus vented. Since the resistive graphite sheets

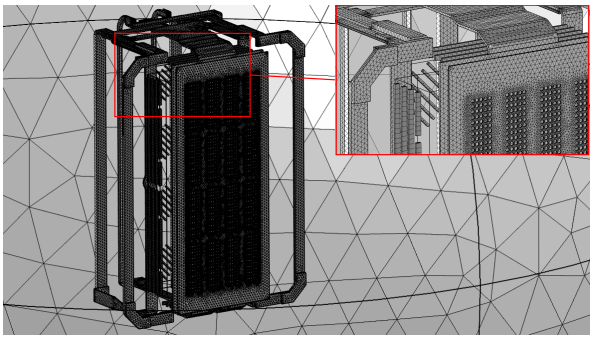

Fig. 6. Mesh with fairly fine overall detail level adopted for the analyses here described; the refined inner box volume is not shown.

proved to work fine in vacuum and not in air, a reduced number of samples was taken in order to not deteriorate the resistive joints. Samples with and without FF current were recorded at different locations, in order to compensate for the intrinsic offset of the probes and also for the field due to the permanent magnets. Samples at the GG surface were also recorded to evaluate the sole intrinsic offset of the probes. The results are discussed in the next paragraph, compared to the numerical simulations.

V. Full Magnetic Model

A complete 3-D magneto-static finite element model (FEM) taking into account all the magnetic field sources has been implemented in Comsol for the first time since SPIDER design [12], thanks to the improvements in the last decade of FEM software and especially of computer performances. Indeed, modeling of current carrying conductors, permanent magnets, and nonlinear magnetic media all together is not a straightforward analysis. In particular, the big size of the overall system, of about 2 m, together with the small size of permanent magnets and grid thickness (lower dimension of 4 mm), and the nonlinear characteristic of the ferromagnetic plate, make the magnetic problem solution computationally demanding. In order to simplify the calculations, the grid apertures were not actually modeled in the FEM dc current model of the PG, but their effect was taken into account by assigning an equivalent resistivity to the regions corresponding to the beamlet groups. This allows getting a globally correct result, losing some detail close to the PG itself. The apertures are instead considered in FEM magnetic model of the ferromagnetic plate, since the nonlinear behavior does not allow determining a single magnetic permeability value equivalent to full-empty ratio, as for the electric resistivity.

Meshes of just under 3 million elements, corresponding to nonlinear systems of nearly 4 million DoFs, could be solved on the available servers. Different models, with localized refinements in specific regions, were run out for a precise mapping of the field in different areas of the plasma source. In Fig. 6, a mesh with a fairly fine overall detail level is shown, used for the analyses reported in the following. An outer sphere of 5 m radius is consider for the boundary conditions and an inner box volume corresponding to the expansion chamber and driver regions is meshed with a higher degree of refinement.

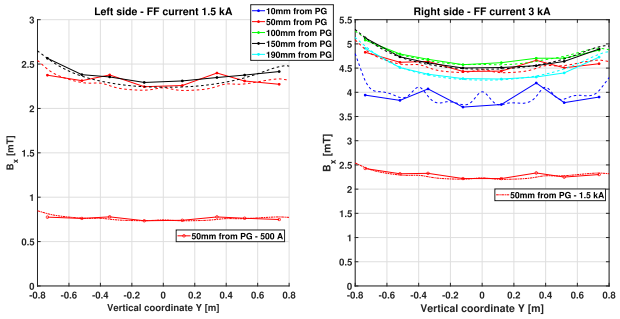

Fig. 7. Comparison of the B_x component of the field measured and calculated along the vertical y-direction for the different z locations sampled, considering the solely FF contribution.

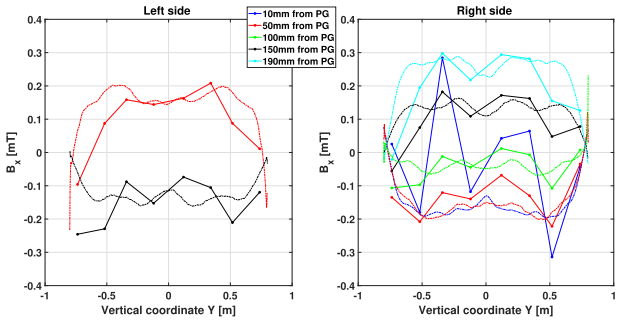

Fig. 8. Comparison of the B_x component of the field measured and calculated along the vertical y-direction for the different z locations sampled, considering the solely permanent magnets contribution.

A. Model-Measurements Benchmark

Primary aim of this activity was to compare measurements and calculated magnetic field. In Fig. 7 the comparison of the horizontal B_x component of the field due to the FF current only is reported. As already mentioned, the measurement data are obtained by subtracting the measures with zero FF current to the measures with a certain current, in order to remove the intrinsic offset and that due to the permanent magnets. On the left side two measurements at 50 mm from the PG where taken with 500 A and 1.5 kA, and one at 150 mm with 1.5 kA. On the right side, all the five z positions were tested at 3 kA and at 50 mm also with 1.5-kA current. A good agreement between measurements and calculations can be observed.

Comparison of the horizontal B_x component of the field due to the permanent magnets contribution only is instead reported in Fig. 8. In this case, the agreement between measurement and calculation is less precise and this can be ascribed to several reasons. First of all, a smaller magnetic field and therefore a lower signal/noise ratio is measured. For this reason, also the effect of a possible probe misalignment is greater and detection of orthogonal magnetic field components gives a major contribution. This is probably, particularly, the case of the measurement at 10 mm from the PG, where a nonnegligible B_y component due to the EGPM is expected. Moreover, in this case, the measurement data are obtained by subtracting the reference measurements taken at the GG surface to the measurements obtained in the actual positions inside the plasma source. Therefore, the measurement offset of the probes probably is not well estimated, because of some

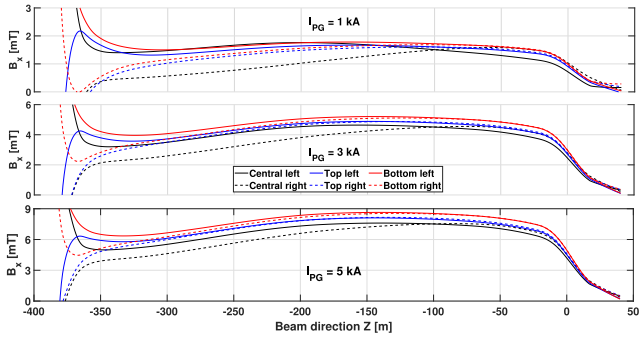

Fig. 9. B_x component on paths along the beam direction z, from the driver back plate to 40-mm downstream of the PG, on central (black), top (blue), bottom (red) apertures, on the left (continuous lines) and right (dotted lines), for 1 kA (top), 3 kA (central), and 5 kA (bottom) FF current.

small contribution of the combined presence of the CPM set and of the iron plate. However, measures and calculations roughly matches also in this case and this is considered to be a further proof that the actual magnetic configuration is as designed, without relevant inconsistency observed.

It is worth noting that the main contribution to the horizontal component of the magnetic field in the plasma source from permanent magnets is due to the LWPM set. Therefore, the LWPMs, together with the vertical non-uniformity due to the connecting paths of the FF current bus-bars, give a relevant contribution to the global magnetic field inside the plasma source, which might be the reason of the left-right asymmetry in the SPIDER plasma performances at high FF currents. This aspect is further analyzed in the next paragraph.

B. Magnetic Field Mapping

Given the good agreement with experimental data, the model has been used to analyze in detail the distribution of the magnetic field. It is possible to attempt to quantify non-uniformity by plotting the components of the field along relevant paths. For instance, in Fig. 9 the B_x component of the field is plotted on paths along the beam direction (z), from the driver backplate up to about the GG, in three vertical positions, both on the left and on the right sides of the source and for three different values of the FF current (1, 3, and 5 kA). Here, it is possible to see that because of the combined presence of the permanent magnets and ferromagnetic plate, the relative magnetic field trend on the different paths changes varying the FF current.

However, in our opinion, the topology of the field is more interesting in order to get any hints on possible reasons of left-right dissimilarities, and between the center and the top-bottom part of the ion source. For this purpose, the horizontal component of the field (B_x and B_z) on horizontal cross sections corresponding to the expansion and driver regions have been analyzed. The magnetic field (absolute value, streamlines, and direction) corresponding to a section in the center of the beamlet groups indicated as 21–24 in Fig. 4, for 1-, 3-, and 5-kA FF current, is plotted in Fig. 10. In Fig. 11 the results for 3-kA FF current on the upper and lower beamlets of beamlet groups 11–14 and 41–44, respectively, are instead reported. It is possible to see the important contribution of the LWPM

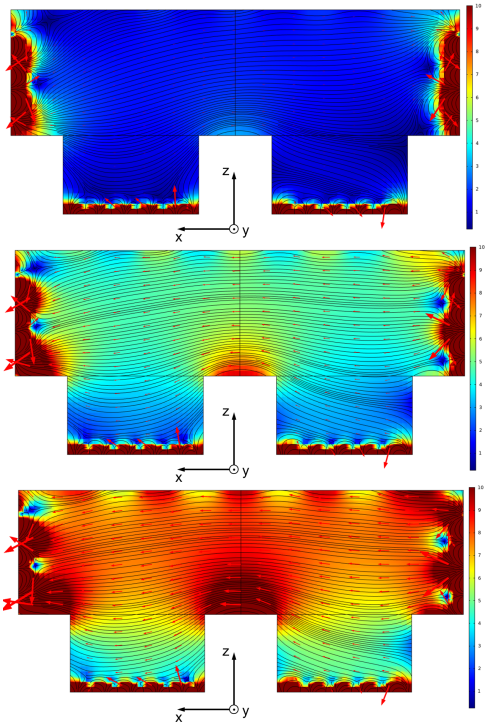

Fig. 10. Magnetic field distribution (absolute value, stream lines and direction) on a horizontal cross section in the center of the beamlet groups indicated as 21–24 in Fig. 4, for 1 (top), 3 (center), and 5 kA (bottom) FF current.

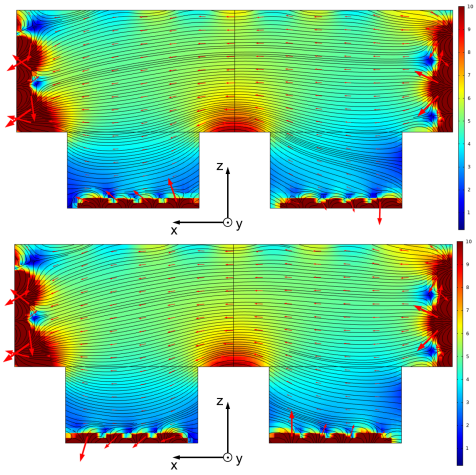

Fig. 11. Magnetic field distribution due to 3-kA FF current on a cross section on the center of beamlet groups 11–14 (top) and 41–44 (bottom), respectively.

set on the overall field distribution, which causes a left-right non-uniformity, both in the driver and expansion region The DBPM set further worsens the uniformity. The non-uniformity does not change that much with the FF current in the center of the source, while greater differences affects the extremities in vertical direction. The field results both stronger and more uneven on the top and bottom parts of the source with respect to the center.

As a confirmation of the results described here, when the FF was inverted during the experimental operations, the plasma non-uniformity caused by the FF was less severe, thanks to

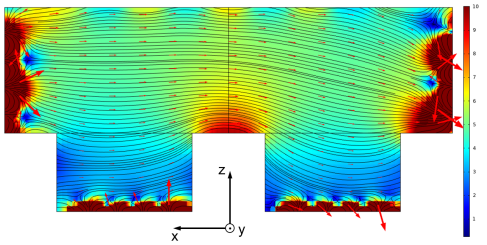

Fig. 12. Magnetic field distribution due to 3-kA FF current with inverted direction on a cross section on the center of beamlet groups 11–14.

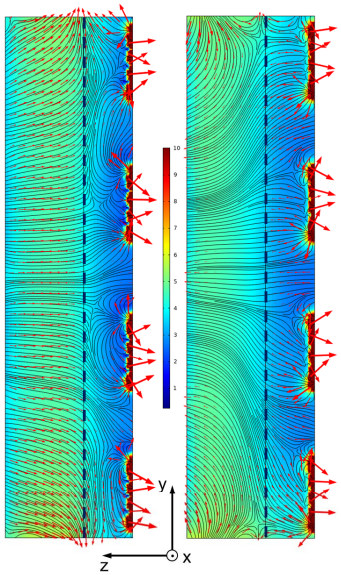

Fig. 13. Magnetic field distribution due to 3-kA FF current on vertical cross sections passing through the central beamlet of beamlet groups 11–41 (left) and 14–44 (right). Vertical dashed lines indicate the plane corresponding to the driver exits. In this case, logarithmic scaling is used for field arrows.

the better interaction between FF and LWPM field [13]. The magnetic field on the upper beamlets of beamlet groups 11–14 for 3-kA FF current with inverted direction is shown in Fig. 12. By comparing this results with Fig. 11, it is possible to notice that the inversion of the FF field, besides mirroring between the left and right side, produces also a top-bottom inversion.

Finally, it is interesting to see the field distribution along vertical cross sections. The vertical component of the field (B_y and B_z) on vertical sections, again through the expansion chamber and driver regions, corresponding to the central beamlet of beamlet groups 11–41 and 14–44, are, respectively, shown on the left and right side of Fig. 13. The figure shows a quite different field structure on the two sides and in particular in the region corresponding to the drivers exit.

However, the complexity of magnetic topology does not allow an *a priori* interpretation of these results. The model presented is indeed used also for extracting precise magnetic field maps to be used in fluid-model-based code for discharge analysis in RF-driven plasma sources [14].

VI. Conclusion

This article presents the numerical and experimental activity carried out in order to assess the actual magnetic field in SPIDER. The recent modifications on the magnetic field configuration, together with asymmetry on the plasma performances observed at high FF, asked for both a routine monitor of the FF current and an *ad hoc* field mapping campaign. A 3-D numerical model, taking into account all magnetic field sources, has been implemented and experimentally benchmarked, allowing a detailed analysis of the complex field structure. The model allows also for a precise mapping of the magnetic field in relevant regions, such as RF drivers and expansion chamber, for further analyses of plasma discharges.

Acknowledgment

The views and opinions expressed herein do not necessarily reflect those of the ITER Organization.

References

[1] G. Serianni *et al.*, "SPIDER in the roadmap of the ITER neutral beams," *Fusion Eng. Des.*, vol. 146, pp. 2539–2546, Sep. 2019, doi: 10.1016/j.fusengdes.2019.04.036.

[2] P. Agostinetti *et al.*, "Physics and engineering design of the accelerator and electron dump for SPIDER," *Nucl. Fusion*, vol. 51, no. 6, Jun. 2011, Art. no. 063004, doi: 10.1088/0029-5515/51/6/063004.

[3] D. Wünderlich *et al.*, "Influence of the magnetic field topology on the performance of the large area negative hydrogen ion source test facility ELISE," *Plasma Phys. Controlled Fusion*, vol. 58, no. 12, Dec. 2016, Art. no. 125005, doi: 10.1088/0741-3335/58/12/125005.

[4] S. Geng *et al.*, "Spatial distributions of charged particles and plasma potential before and during beam extraction in a negative hydrogen ion source for NBI," *Plasma Fusion Res.*, vol. 10, Mar. 2015, Art. no. 3405016, doi: 10.1585/pfr.10.3405016.

[5] S. Mori and O. Fukumasa, "D/H negative ion production versus plasma parameters in a volume negative ion source," *Rev. Sci. Instrum.*, vol. 79, no. 2, 2008, Art. no. 02A507, doi: 10.1063/1.2802594.

[6] V. Toigo *et al.*, "The PRIMA test facility: SPIDER and MITICA testbeds for ITER neutral beam injectors," *New J. Phys.*, vol. 19, no. 8, Aug. 2017, Art. no. 085004, doi: 10.1088/1367-2630/aa78e8.

[7] G. Serianni *et al.*, "First operation in SPIDER and the path to complete MITICA," *Rev. Sci. Instrum.*, vol. 91, no. 2, Feb. 2020, Art. no. 023510, doi: 10.1063/1.5133076.

[8] N. Marconato *et al.*, "An optimized and flexible configuration for the magnetic filter in the SPIDER experiment," *Fusion Eng. Des.*, vol. 166, May 2021, Art. no. 112281, doi: 10.1016/j.fusengdes.2021.112281.

[9] V. Toigo *et al.*, "On the road to ITER NBIs: SPIDER improvement after first operation and MITICA construction progress," *Fusion Eng. Des.*, vol. 168, Jul. 2021, Art. no. 112622, doi: 10.1016/j.fusengdes.2021.112622.

[10] A. Pimazzoni *et al.*, "Co-extracted electrons and beam inhomogeneity in the large negative ion source SPIDER," *Fusion Eng. Des.*, vol. 168, Jul. 2021, Art. no. 112440, doi: 10.1016/j.fusengdes.2021.112440.

[11] G. Chitarin *et al.*, "Improvements of the magnetic field design for SPIDER and MITICA negative ion beam sources," *AIP Conf.*, vol. 1655, Apr. 2015, Art. no. 040008, doi: 10.1063/1.4916450.

[12] N. Marconato, G. Chitarin, P. Agostinetti, N. Pilan, and G. Serianni, "Simulation, code benchmarking and optimization of the magnetic field configuration in a negative ion accelerator," *Fusion Eng. Des.*, vol. 86, nos. 6–8, pp. 925–928, Oct. 2011, doi: 10.1016/j.fusengdes.2011.01.052.

[13] E. Sartori *et al.*, "First operations with caesium of the negative ion source SPIDER," *Nucl. Fusion*.

[14] R. Zagorski *et al.*, "2D fluid-model for discharge analysis of the RF-driven prototype ion source for ITER NBI (SPIDER)," *IEEE Trans. Plasma Sci.*

Open Access funding provided by 'Università degli Studi di Padova' within the CRUI-CARE Agreement